



Topology optimization with linearized buckling criteria in 250 lines of Matlab

Ferrari, Federico; Sigmund, Ole; Guest, James K.

Published in:
Structural and Multidisciplinary Optimization

Link to article, DOI:
[10.1007/s00158-021-02854-x](https://doi.org/10.1007/s00158-021-02854-x)

Publication date:
2021

Document Version
Peer reviewed version

[Link back to DTU Orbit](#)

Citation (APA):
Ferrari, F., Sigmund, O., & Guest, J. K. (2021). Topology optimization with linearized buckling criteria in 250 lines of Matlab. *Structural and Multidisciplinary Optimization*, 63, 3045–3066. <https://doi.org/10.1007/s00158-021-02854-x>

General rights

Copyright and moral rights for the publications made accessible in the public portal are retained by the authors and/or other copyright owners and it is a condition of accessing publications that users recognise and abide by the legal requirements associated with these rights.

- Users may download and print one copy of any publication from the public portal for the purpose of private study or research.
- You may not further distribute the material or use it for any profit-making activity or commercial gain
- You may freely distribute the URL identifying the publication in the public portal

If you believe that this document breaches copyright please contact us providing details, and we will remove access to the work immediately and investigate your claim.

Topology Optimization with linearized buckling criteria in 250 lines of Matlab

Federico Ferrari · Ole Sigmund · James K. Guest

Published in: *Structural and Multidisciplinary Optimization* 63, 3045-3066 (2021)

Abstract We present a 250 line Matlab code for topology optimization for linearized buckling criteria. The code is conceived to handle stiffness, volume and Buckling Load Factors (BLFs) either as the objective function or as constraints. We use the Kreisselmeier-Steinhauser aggregation function in order to reduce multiple objectives (viz. constraints) to a single, differentiable one. Then, the problem is sequentially approximated by using MMA-like expansions and an OC-like scheme is tailored to update the variables. The inspection of the stress stiffness matrix leads to a vectorized implementation for its efficient construction and for the sensitivity analysis of the BLFs. This, coupled with the efficiency improvements already presented by Ferrari and Sigmund (2020a), cuts all the computational bottlenecks associated with setting up the buckling analysis and allows buckling topology optimization problems of an interesting size to be solved on a laptop. The efficiency and flexibility of the code is demonstrated over a few structural design examples and some ideas are given for possible extensions.

Keywords Topology optimization · Matlab · Buckling optimization · Aggregation functions · Optimality criteria

1 Introduction

We present a compact code aimed at reducing the burden of a computationally intensive task: topology optimization considering buckling performed in Matlab.

Topology Optimization (TO) is actively spreading across several engineering fields, offering innovative solutions to more and more design problems. Most likely, one of the driving forces of this rapid spreading is the availability of much educational software. We believe that educational software is a highly valuable tool, offering a foundation for the understanding of the basics of a research topic and providing a basis for the implementation (and improvement) of methods. Since the forefather 99 line code by Sigmund (2001), many others educational codes have appeared (see Ferrari and Sigmund (2020a) for a list), almost all addressing the prototypical problems of compliance (thermal or elastic) design and mechanism design. In recent years, more TO problems have been translated into educational software, addressing different physics (Xia and Breitkopf, 2015), design parametrizations (Yago et al, 2021), and sometimes making use of external FEM libraries for the most computationally intensive tasks.

Confining ourselves to density-based TO (Bendsøe and Sigmund, 2004) and to structural applications, almost all educational codes deal with compliance design and we observe the lack of any software addressing buckling. This is understandable, as buckling TO is still an advanced topic, presenting several difficulties (Bruyneel et al, 2008; Ferrari and Sigmund, 2019), even in its linearized formulation (Crisfield, 1991). Within the Matlab environment, buckling analysis is computationally demanding not only due to the eigenproblem solution (progress has been made by using multi-level solvers for this (Ferrari and Sigmund, 2020b)), but

F. Ferrari · James K. Guest
Department of Civil and Systems Engineering
Johns Hopkins University
Latrobe Hall, 21218 Baltimore MD, USA
E-mail: fferrar3@jhu.edu; jkguest@jhu.edu

O. Sigmund
Department of Mechanical Engineering
Technical University of Denmark
Nils Koppels Allé 404, 2800 Kongens Lyngby, Denmark
E-mail: sigmund@mek.dtu.dk

also due to the stress stiffness matrix setup. The latter depends on the local stress distribution, and therefore its customary setup requires potentially time consuming elementwise operations. Based on the direct inspection of the stress stiffness operator, we provide an almost fully vectorized implementation eliminating all the computational bottlenecks associated with the setup of the buckling problem and with the sensitivity analysis of the Buckling Load Factors (BLFs).

The code we present, named `topBuck250`, solves TO problems involving a combination of compliance, volume and BLFs. Therefore, it stands as a quite comprehensive design tool, accounting for the most relevant structural responses. In particular, the code in Appendix C is ready to tackle the following problems

1. Maximization of the fundamental BLF of a design, subject to compliance and volume constraints,
2. Minimum volume design, subject to compliance and buckling constraints,

that are highly meaningful for structural designers.

We aggregate multiple objectives or constraints by using the Kreisselmeier-Steinhauser (KS) function (Kreisselmeier and Steinhauser, 1979), which has proven very robust when dealing with many active constraints (Kennedy and Hicken, 2015; Ferrari and Sigmund, 2019). The single objective, single constraint optimization problem is then solved by a sequential approximation approach, using monotonic MMA-like approximations (Svanberg, 1987) and an OC-like scheme to update the variables. For this, we provide a very compact re-design routine, tailored for solving the specific problems here discussed.

The present code builds on the recently published `top99neo` code (Ferrari and Sigmund, 2020a) and inherits all its basic speedups (i.e. fast assembly implementation, use of volume-preserving filters, etc.). Thus, the solution of the eigenproblem will absorb the majority of the computational time and a highly efficient eigensolver (Dunning et al, 2016; Ferrari and Sigmund, 2020b) could be used to improve this operation. We do not provide here a complete 3D implementation, because *the solution* of the 3D eigenproblem would quickly become prohibitive with the built-in Matlab tools. Nevertheless, all the methods discussed here are easily extendable to 3D and we will show the huge cut in the CPU time they potentially bring in that setup. Also, the methods presented can be extended to some other discretizations, e.g. higher order isoparametric elements, some mixed elements and level sets.

The paper is organized as follows. In Section 2 we set the stage for density-based TO, introducing the physical responses of interest and their sensitivities. Subsection 2.1 introduces the optimization problems considered and qualitatively describes the solution scheme.

Section 3 gives an overview of the organization of the `topBuck250` code and describes the input parameters. The efficient construction of the stress stiffness matrix and the corresponding sensitivity analysis of the BLFs are presented in Section 4. Subsection 4.3 gives some information about how the state and adjoint equations are solved. Two examples, immediately replicable with the provided code, are presented in Section 5 and final remarks and possible extensions are listed in Section 6. In Appendix A we explain how some discretization operators have been compactly implemented in the code and Appendix B describes the MMA-like approximation of the local optimization problem and the OC-like update rule. Appendix C provides the Matlab code.

2 Setup and formulations

We consider a structured discretization Ω_h of m equi-sized elements Ω_e for a total of n Degrees of Freedom (DOFs). The pseudo-densities $\hat{\mathbf{x}} = \{\hat{x}_e\}_{e=1}^m$, are partitioned between the sets $\hat{\mathbf{x}}_{\mathcal{P}_0}$, $\hat{\mathbf{x}}_{\mathcal{P}_1}$, describing passive regions where $\hat{x}_e = 0$ and $\hat{x}_e = 1$, respectively, and the active variables set $\hat{\mathbf{x}}_{\mathcal{A}}$ (Ferrari and Sigmund, 2020a). For the latter, \hat{x}_e is linked to the element-based design variables $\mathbf{x} = \{x_e\}_{e=1}^m$ by (Wang et al, 2011)

$$\hat{x}_e = \frac{\tanh(\beta\eta) + \tanh(\beta(\hat{x}_e - \eta))}{\tanh(\beta\eta) + \tanh(\beta(1 - \eta))} \quad (1)$$

where $\eta \in [0, 1]$, $\beta \in [1, \infty)$ and \tilde{x}_e is obtained through the linear density filter with minimum radius $r_{\min} > 0$ (Bourdin, 2001; Bruns and Tortorelli, 2001)

$$\tilde{x}_e = \frac{\sum_{i=1}^m h_{e,i} x_i}{\sum_{i=1}^m h_{e,i}} \quad (2)$$

where $h_{e,i} = \max(0, r_{\min} - \text{dist}(\Omega_i, \Omega_e))$, for all $i, e \in [1, m]$.

Let the Young's modulus be parametrized by the SIMP interpolations with penalizations $p_K, p_G > 1$

$$\begin{aligned} E_K(\hat{x}_e) &= E_{\min} + (E_0 - E_{\min})\hat{x}_e^{p_K} \\ E_G(\hat{x}_e) &= E_0\hat{x}_e^{p_G} \end{aligned} \quad (3)$$

for stiffness (E_K) and stress (E_G), respectively. As usual, E_0 is the Young's modulus of the solid material and $E_{\min} \ll E_0$ that of the void.

We consider the following physical quantities: total volume fraction ($|\Omega_e| = \text{constant}$)

$$f(\hat{\mathbf{x}}) = \frac{1}{m} \sum_{e=1}^m \hat{x}_e, \quad (4)$$

linearized compliance

$$c(\hat{\mathbf{x}}) = \mathbf{F}^T \mathbf{u}(\hat{\mathbf{x}}), \quad (5)$$

and fundamental Buckling Load Factor (BLF)

$$\lambda_1(\hat{\mathbf{x}}, \mathbf{u}) := \min_{\mathbf{v} \in \mathbb{R}^n, \mathbf{v} \neq \mathbf{0}} - \frac{\mathbf{v}^T K[\hat{\mathbf{x}}] \mathbf{v}}{\mathbf{v}^T G[\hat{\mathbf{x}}, \mathbf{u}] \mathbf{v}} \quad (6)$$

The latter two both refer to the same load vector $\mathbf{F} \in \mathbb{R}^n$, that is assumed to have *fixed* direction; therefore, we only consider positive BLFs. $G[\hat{\mathbf{x}}, \mathbf{u}]$ is the stress stiffness matrix, depending on the displacement field $\mathbf{u}(\hat{\mathbf{x}}) = K[\hat{\mathbf{x}}]^{-1} \mathbf{F}$, and $K[\hat{\mathbf{x}}]$ is the linear stiffness matrix.

In the following we will actually compute the quantities $\mu_i = 1/\lambda_i$, which are the eigenvalues of

$$(G[\hat{\mathbf{x}}, \mathbf{u}] + \mu K[\hat{\mathbf{x}}]) \boldsymbol{\varphi} = \mathbf{0}, \quad \boldsymbol{\varphi} \neq \mathbf{0} \quad (7)$$

such that $\mu_1 = \max \mu_i = 1/\min \lambda_i = 1/\lambda_1$. Then, the max operator is approximated by the smooth aggregation function (Kreisselmeier and Steinhauser, 1979)

$$J^{KS}[\mu_i](\hat{\mathbf{x}}) = \mu_1(\hat{\mathbf{x}}) + \frac{1}{\rho} \ln \left(\sum_{i=1}^q e^{\rho(\mu_i(\hat{\mathbf{x}}) - \mu_1(\hat{\mathbf{x}}))} \right) \quad (8)$$

depending on $\rho \in [1, \infty)$ and giving an upper bound on μ_1 (thus, a lower bound on λ_1).

The derivatives of the compliance and volume fraction with respect to the pseudo-densities \hat{x}_e are

$$\frac{\partial c}{\partial \hat{x}_e} = -\mathbf{u}^T \frac{\partial K}{\partial \hat{x}_e} \mathbf{u} \delta_{eA}, \quad \frac{\partial f}{\partial \hat{x}_e} = m^{-1} \delta_{eA} \quad (9)$$

where $\delta_{eA} = 1$ if $e \in A$ and 0 otherwise. The derivatives of the i -th eigenvalue reads (Rodríguez et al, 1995)

$$\frac{\partial \mu_i}{\partial \hat{x}_e} = - \underbrace{[\boldsymbol{\varphi}_i^T \frac{\partial G}{\partial \hat{x}_e} \boldsymbol{\varphi}_i]}_{\textcircled{1}} + \mu_i \underbrace{\boldsymbol{\varphi}_i^T \frac{\partial K}{\partial \hat{x}_e} \boldsymbol{\varphi}_i}_{\textcircled{2}} - \underbrace{\mathbf{w}_i^T \frac{\partial K}{\partial \hat{x}_e} \mathbf{u}}_{\textcircled{3}} \quad (10)$$

where $\mathbf{w}_i = K^{-1}[\boldsymbol{\varphi}_i^T (\nabla_{\mathbf{u}} G) \boldsymbol{\varphi}_i]$ is the adjoint vector, and the derivative of (8) is (Raspanti et al, 2000)

$$\frac{\partial J^{KS}[\mu_i]}{\partial \hat{x}_e}(\hat{\mathbf{x}}) = \frac{\sum_{i=1}^q e^{\rho(\mu_i(\hat{\mathbf{x}}) - \mu_1(\hat{\mathbf{x}}))} \frac{\partial \mu_i}{\partial \hat{x}_e}(\hat{\mathbf{x}})}{\sum_{i=1}^q e^{\rho(\mu_i(\hat{\mathbf{x}}) - \mu_1(\hat{\mathbf{x}}))}} \quad (11)$$

We remark that (11) is smooth even at design points where some of the $\partial_e \mu_i$ are not (Gravesen et al, 2011), i.e. points where μ_i are repeated (Seyranian et al, 1994).

With (9) and (11) in hand, sensitivities with respect to the design variables x_e , are given by the chain rule

$$\frac{\partial(\cdot)}{\partial x_e} = \frac{\partial(\cdot)}{\partial \hat{x}_e} \frac{\partial \hat{x}_e}{\partial x_e} \quad (12)$$

(\cdot) may represent c , f or J^{KS} and the rightmost terms involve derivatives of the projection (1) and filtering (2) operators (Guest et al, 2004; Sigmund, 2007).

2.1 Optimization problems and solution approach

The code in Appendix C solves the following problems: (1) BLF maximization with compliance and volume constraints (recall that $J_0^{KS}[\mu_i]$ is linked to $1/\lambda_1$),

$$\begin{cases} \min_{\mathbf{x} \in [0,1]^m} J_0^{KS}[\mu_i](\hat{\mathbf{x}}) \\ \text{s.t. } J_1^{KS}[g_V, g_c](\hat{\mathbf{x}}) \leq 0 \end{cases} \quad (13)$$

and (2) volume minimization with compliance and BLF constraints

$$\begin{cases} \min_{\mathbf{x} \in [0,1]^m} f(\hat{\mathbf{x}}) \\ \text{s.t. } J_1^{KS}[g_c, g_\lambda](\hat{\mathbf{x}}) \leq 0 \end{cases} \quad (14)$$

where we used the KS function to aggregate multiple constraints (see Appendix B). Explicitly, the constraint functions that are aggregated in (13) and (14) are

$$\begin{aligned} g_V(\hat{\mathbf{x}}) &= f(\hat{\mathbf{x}})/\bar{f} - 1 \\ g_c(\hat{\mathbf{x}}) &= c(\hat{\mathbf{x}})/\bar{c} - 1 \\ g_\lambda(\hat{\mathbf{x}}) &= 1 - \underline{\lambda} J^{KS}[\mu_i](\hat{\mathbf{x}}) \end{aligned} \quad (15)$$

where \bar{c} and \bar{f} are the maximum allowed compliance and volume fraction and $\underline{\lambda}$ is the minimum prescribed BLF. The two more basic TO problems of volume-constrained minimum compliance and *vice versa* can also be solved (see Section 3).

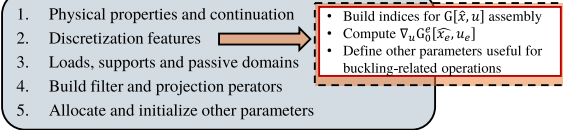
The optimization problems are solved by a sequential approximation approach (Groenwold and Etman, 2008). At each re-design step, the objective and constraint functions are replaced by their monotonic MMA-like approximations (Svanberg, 1987) and the design update is performed within the routine `ocUpdate` listed in Appendix B. Although introducing moving asymptotes and adaptive move limits results in some extra parameters and operations, for the present problems the design update retains the simplicity of an OC-like scheme and can be implemented very compactly.

Because of its simplicity, the `ocUpdate` cannot be expected to be as robust as more general optimization routines, such as the MMA (Svanberg, 1987) or GCMMA (Svanberg, 2002). Therefore, we decided to keep this routine separate from the main code, such that the user can easily switch to other, more general and established optimizers as needed. Details on how to call the MMA within the main code are given in Appendix B.

3 General structure of the code

The code is called with the following input data

Preliminary operations



Re-design Loop: while loop < maxit

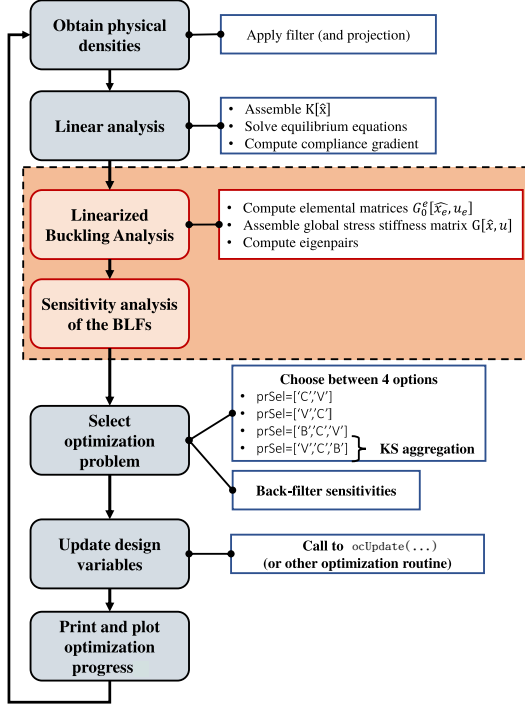


Fig. 1: Flowchart for the `topBuck250` Matlab code. All the operations related to buckling (highlighted with an orange background) are performed only if 'B' is among the argument of `prSel`, otherwise the code essentially reduces to the `top99neo`. The design variables are updated by the routine `ocUpdate`

```
topBuck250(nelx,nely,penalK,rmin,ft,ftBC,eta,beta,
maxit,ocPar,Lx,penalG,nEig,pAgg,prSel,x0)
```

where the first 9 arguments have the same meaning as in `top99neo` (Ferrari and Sigmund, 2020a). `ocPar` contains the parameters governing the design update routine, and will be discussed in Appendix B.

We introduce the physical length of the domain L_x and the height is obtained by the aspect ratio (line 11). `penalG` is the penalization factor used for the stress stiffness interpolation (3), `nEig` is the number of BLFs included in the optimization and `pAgg` is the initial value of the KS aggregation factor.

`prSel` is a data structure specifying the optimization problem and the corresponding constraints bounds. This can take the forms

```
prSel=[['B','C','V'],[Cmax,Vfmax]];
prSel=[['V','C','B'],[Cmax,Lmin]];
```

```
prSel=[['C','V'],Vfmax];
prSel=[['V','C'],Cmax];
```

The first substructure `prSel{1}` is a list of 2 or 3 characters, used to select the optimization problem to be solved. The first character defines the objective function and the other(s) the constraint(s), among the criteria introduced in Section 2. By convention, we set 'B' for the BLF, 'C' for compliance and 'V' for volume fraction. If 'B' is not among the set of arguments, all the buckling-related operations are skipped and we essentially recover the `top99neo` code, except for the `ocUpdate` routine (see Figure 1). In this case, volume-constrained minimum compliance (`prSel{1}=['C','V']`) and compliance-constrained minimum volume (`prSel{1}=['V','C']`) TO problems can be solved with essentially the same efficiency as in `top99neo`. Problems (13) and (14) are selected by setting `prSel{1} = ['B','C','V']` and `prSel{1} = ['V','B','C']`, respectively.

The second substructure `prSel{2}` contains 1 or 2 numerical values, specifying the constraint(s) bound(s) \bar{c} , \bar{f} , $\underline{\lambda}$. We assume the following: (1) for volume minimization problems (i.e. if `prSel{1}(1)='V'`) the initial volume fraction is set to $f = 1$ (see line 9); (2) for volume constrained problems, the maximum volume fraction is specified by `prSel{2}(end)=Vfmax`; (3) the compliance upper bound is expressed as a scaling of the initial compliance (e.g., `Cmax=2.5` means $\bar{c} = 2.5(\mathbf{F}^T \mathbf{u})|_{loop=1}$).

The last argument is a string with the name of a data file (e.g. `'myData.mat'`), and can be used to specify a non-uniform initial material distribution. This is useful for solving reinforcement problems starting from an initial design (see Subsection 5.1). We assume that the material distribution is saved as `"xInitial"` in the data file, and then is assigned to the design variables on line 91 in the code. If this last argument is not passed to `topBuck250`, the design variables vector is initialized to the uniform material distribution fulfilling the specified volume fraction `volfrac` (see lines 93-94).

The `topBuck250` routine starts with some preliminary operations subdivided in the following blocks

```
PRE.1) MATERIAL AND CONTINUATION PARAMETERS
PRE.2) DISCRETIZATION FEATURES
PRE.3) LOADS, SUPPORTS AND PASSIVE DOMAINS
PRE.4) PREPARE FILTER AND PROJECTION OPERATORS
PRE.5) ALLOCATE AND INITIALIZE OTHER PARAMETERS
```

We first define the elastic constants, the continuation schemes for the penalization exponents (`penalK`, `penalG`), for the projection parameter `beta` and for the aggregation exponent `pAgg` (lines 3-7). We remark that, as in `top99neo`, the continuation scheme on a given parameter is specified as

```
parCont={istart,maxPar,isteps,deltaPar};
```

such that when `loop>=istart`, the parameter is increased by `deltaPar` every `isteps`, up to the value `maxPar`. The continuation is applied at lines 245-246, by the function defined on line 8. The check on lines 247-248 keeps track of the steps where continuation is applied, and allows the user to restart the asymptotes history (see Appendix B).

The discretization features are built between lines 11-59. Up to line 32 the operations are the same as in `top99neo`, and we remark that the indices `iK` and `jK`, used for the K matrix assembly (lines 27-32), refer to the lower-half of the symmetric matrix and are built as explained in Ferrari and Sigmund (2020a).

Lines 33-62 are executed only if buckling is among the optimization criteria. We introduce the non dimensional elasticity matrix `Cmat0`, the physical dimensions of the elements `xe`, and the Gauss nodes (`xiG,etaG`) and weights (`wxi,weta`) adopted for numerical quadratures (lines 34-36). Some operators useful in order to compactly perform the stress analysis are introduced in lines 37-39 (see Appendix A for details). The indices `iG` and `jG` used for the stress stiffness matrix assembly, the derivative of this latter with respect to the displacement vector, and other auxiliary variables are defined between lines 40-59. These operations are all precisely discussed in Section 4.

The KS function and its derivative, as specified by (8) and (11) are defined as functions on lines 60 and 61. The specification of loads, boundary conditions and passive elements follows the same concept of `top88` and `top99neo`, and the instructions given by default on lines 64-69 correspond to the compressed column example of Subsection 5.1.

The filter operator is built in `PRE.4`, using Dirichlet (`bcF='D'`) or Neumann (`bcF='N'`) boundary conditions, and lines 78-83 define the η projection (`prj`) and its η - and \hat{x}_e -derivatives (`deta,dprj`). Block `PRE.5` is basically as in `top99neo`. The only notable difference is that lines 90-95 allow the user to initialize the design variables to the initial guess specified by `x0`, or to the uniform material distribution.

The redesign loop starts at line 98 and consists of the following blocks

```

RL.1) COMPUTE PHYSICAL DENSITY FIELD
RL.2) SETUP AND SOLVE EQUILIBRIUM EQUATIONS
RL.3) BUILD STRESS STIFFNESS MATRIX
RL.4) SOLVE BUCKLING EIGENVALUE PROBLEM
RL.5) SENSITIVITY ANALYSIS OF BLFs
RL.6) SELECT OBJECTIVE FUNCTION AND CONSTRAINTS
RL.7) UPDATE DESIGN VARIABLES
RL.8) PRINT AND PLOT RESULTS

```

`RL.1`) and `RL.2`) perform the operations needed for computing the linear compliance and its derivative. The operations in blocks `RL.3`) to `RL.5`) are discussed in detail in Section 4 and are executed only if buckling is

among the optimization criteria (see Figure 1). Such a modular organization of the code allows the user to skip the most computationally intensive parts if the purpose is to solve standard compliance or volume minimization problems, e.g in order to generate an initial design to be then reinforced against buckling.

Up to this point the script has the greatest generality and, depending on the problem selected, provides the function values and gradients for the three physical responses: compliance, volume fraction and μ_i parameters, that are related to BLFs. Then, `RL.6`) and `RL.7`) are customized for the particular optimization problems introduced in Subsection 2.1 and for performing the design update with the `ocUpdate` routine, as described in Appendix B. However, we remark that the extension of the code for considering other combinations of the three response criteria, as well as for using more general optimization routines, requires the user to add/modify only a few lines in `RL.6`) and `RL.7`).

The last block (`RL.8`) contains some commands for print and plot. If buckling is selected, lines 231-238 generate three sub-plots. The top one shows the current topology, the bottom left one shows the evolution of the constraint functions, together with their KS aggregation, and the evolution of the objective (volume fraction or $J^{KS}[\mu_i]^{-1}$). The bottom right plot shows the evolution of the four lowest BLFs, respectively. Otherwise, if buckling is not selected, a single plot showing the evolution of the design is generated.

4 Setup of the buckling eigenvalue problem and sensitivity analysis of buckling load factors

In order to setup the eigenvalue buckling analysis (7) we need to assemble the stress stiffness matrix $G[\hat{\mathbf{x}}, \mathbf{u}]$ from the elemental ones $G^e[\hat{x}_e, \mathbf{u}_e]$, $e = 1 \dots, m$.

The elemental matrices cannot be expressed as a scaling of a constant matrix (like $K^e = E_K(\hat{x}_e)K_0^e$), but must be evaluated for each element, as they depend on the local displacement field. Within a scripting language such as Matlab, where loops and memory allocation considerably affect the performance, this becomes very expensive even for medium-size problems. However, a careful inspection of the structure of $G^e[\hat{x}_e, \mathbf{u}_e]$ allows a very efficient implementation, requiring cheap vectorized matrix products only.

The first step is to compute the stress components $\sigma_x^e, \sigma_y^e, \tau_{xy}^e$ at the element level, and arrange them into the matrix $\boldsymbol{\sigma}_0^e$. For a k -noded isoparametric element (Zienkiewicz and Taylor, 2005) this is done through the following relationship

$$\boldsymbol{\sigma}_0^e = DB_0 \mathbf{u}^e \quad (16)$$

where D is the elasticity matrix and B_0 is the linearized strain-displacement pseudo-differential operator.

Using the operators defined in Appendix A, Equation 16 is evaluated simultaneously for all the elements by the following two lines

```
% ----- stress at current Gauss point (nElemx3)
gradN = (dN(0,0)*xe)\dN(0,0);
sGP = (Cmat0*Bmat(gradN)*U(cMat)')';
```

where the element centroid is the stress super-convergent point for the \mathcal{Q}_4 bilinear element (Wahlbin, 1995).

4.1 Setup of the stress stiffness matrix

The stress stiffness matrix stems from the following contribution in the linearization of the virtual work equation (Zienkiewicz and Taylor, 2005)

$$G^e[\mathbf{u}_e] := \int_{\Omega_0} B_1^T \mathbb{T}[\boldsymbol{\sigma}_0^e] B_1 \, d\Omega_0 \quad (17)$$

where B_1 discretizes the deformation gradient and for a \mathcal{Q}_4 bilinear element reads (Crisfield, 1991)

$$B_1 = \begin{bmatrix} \partial_x N_1 & 0 & \partial_x N_2 & 0 & \partial_x N_3 & 0 & \partial_x N_4 & 0 \\ \partial_y N_1 & 0 & \partial_y N_2 & 0 & \partial_y N_3 & 0 & \partial_y N_4 & 0 \\ 0 & \partial_x N_1 & 0 & \partial_x N_2 & 0 & \partial_x N_3 & 0 & \partial_x N_4 \\ 0 & \partial_y N_1 & 0 & \partial_y N_2 & 0 & \partial_y N_3 & 0 & \partial_y N_4 \end{bmatrix}$$

and the stress components are arranged as

$$\mathbb{T}[\boldsymbol{\sigma}_0^e] = I_2 \otimes \boldsymbol{\sigma}_0^e = \begin{bmatrix} \sigma_x & \tau_{xy} & 0 & 0 \\ \tau_{xy} & \sigma_y & 0 & 0 \\ 0 & 0 & \sigma_x & \tau_{xy} \\ 0 & 0 & \tau_{xy} & \sigma_y \end{bmatrix} \quad (18)$$

where I_2 is the identity matrix of order 2.

Expanding the product $B_1^T \mathbb{T}[\boldsymbol{\sigma}_0^e] B_1$ we obtain the following structure for the integrand of (17) (de Borst et al, 2012)

$$G_{\{\mathcal{Q}_4\}}^e = \begin{bmatrix} z_{11} & 0 & z_{12} & 0 & z_{13} & 0 & z_{14} & 0 \\ 0 & z_{11} & 0 & z_{12} & 0 & z_{13} & 0 & z_{14} \\ z_{21} & 0 & z_{22} & 0 & z_{23} & 0 & z_{24} & 0 \\ 0 & z_{21} & 0 & z_{22} & 0 & z_{23} & 0 & z_{24} \\ z_{31} & 0 & z_{32} & 0 & z_{33} & 0 & z_{34} & 0 \\ 0 & z_{31} & 0 & z_{32} & 0 & z_{33} & 0 & z_{34} \\ z_{41} & 0 & z_{42} & 0 & z_{43} & 0 & z_{44} & 0 \\ 0 & z_{41} & 0 & z_{42} & 0 & z_{43} & 0 & z_{44} \end{bmatrix} \quad (19)$$

and we identify only 10 independent coefficients out of the 64, highlighted in red in (19). Moreover, the generic z_{ik} ($i, k = 1, \dots, 4$) can be expressed as a linear combination of the stress components

$$z_{ik} = \sigma_x a_k a_i + \sigma_y b_k b_i + \tau_{xy} (b_k a_i + a_k b_i) \quad (20)$$

	1	2	3	4	5	6	7	8	9	10
\mathcal{M}_{odd}	(1,1)	(3,1)	(5,1)	(7,1)	(3,3)	(5,3)	(7,3)	(5,5)	(7,5)	(7,7)
$\mathcal{M}_{\text{even}}$	(2,2)	(4,2)	(6,2)	(8,2)	(4,4)	(6,4)	(8,4)	(6,6)	(8,6)	(8,8)

Table 1: Mapping $\mathcal{M}_{\text{odd}} : \{1 : 10\} \mapsto (i, j)$ for the 10 unique coefficients of \mathbf{Z} and the *lower* symmetric part of G^e . $\mathcal{M}_{\text{even}}$ in the second row is for even columns

where we have set $a_i = \partial_x N_i$ and $b_i = \partial_y N_i$.

A compact representation of the 10 independent coefficients in (19) is given by the array $\mathbf{Z} \in \mathbb{R}^{m \times 10}$, which is obtained through the Hadamard matrix product $\mathbf{Z} = \mathbf{B}^T \odot \mathbf{S}$. Here, $\mathbb{R}^{m \times 3} \ni \mathbf{S} = [\sigma_x^e, \sigma_y^e, \tau_{xy}^e]_{e=1:m}$ collects the stress components for all the elements, and we have introduced the array $\mathbf{B}_{[3 \times 10]}$

$$\mathbf{B} = \begin{bmatrix} a_{\ell(i,1)} a_{\ell(i,2)} \\ b_{\ell(i,1)} b_{\ell(i,2)} \\ b_{\ell(i,2)} a_{\ell(i,1)} + a_{\ell(i,2)} b_{\ell(i,1)} \end{bmatrix}^{i=1:10} \quad (21)$$

where $\ell \in \mathbb{N}^{10 \times 2}$ is the set of indices mapping each \mathbf{Z}_{ei} ($i = 1, \dots, 10$) to the corresponding $z_{\ell(i,1)\ell(i,2)}$ within the pattern of non-zero elements of (19), i.e.

$$\ell = \begin{bmatrix} 1 & 2 & 3 & 4 & 2 & 3 & 4 & 3 & 4 & 4 \\ 1 & 1 & 1 & 1 & 2 & 2 & 2 & 3 & 3 & 4 \end{bmatrix}^T$$

The columns of \mathbf{Z} collect the coefficients highlighted in the reduced pattern here below, sorted column-wise

$$G_{\{\mathcal{Q}_4\}}^{e,\text{unique}} = \begin{bmatrix} z_{11} & z_{12} & z_{13} & z_{14} \\ z_{21} & z_{22} & z_{23} & z_{24} \\ z_{31} & z_{32} & z_{33} & z_{34} \\ z_{41} & z_{42} & z_{43} & z_{44} \end{bmatrix} \quad (22)$$

Thus, we obtain the independent stress stiffness matrix coefficients for all the elements at once, and we just need a small loop to evaluate \mathbf{Z} on the Gauss points. We remark that \mathbf{Z} actually contains non-dimensional strain combinations, and K_0^e and G_0^e are scaled by the interpolations $E_K(\hat{x}_e)$ and $E_G(\hat{x}_e)$, to obtain the dimensional matrices K^e and G^e , right before the global assembly. The whole procedure for arriving at $G[\hat{\mathbf{x}}, \mathbf{u}]$ is implemented between lines 124-148.

The global stress stiffness matrix G can be assembled as discussed by Ferrari and Sigmund (2020a), upon considering the mapping \mathcal{M}_{odd} between the 10 columns of \mathbf{Z} and the *odd* columns of the *lower* symmetric part of G^e (see Table 1). Mapping to *even* columns is then easily obtained by noting that $(i, j)_{\text{even}} = (i, j)_{\text{odd}} + (1, 1)$, and gives the coefficients highlighted in cyan in (19). The indices iG and jG are subsets of iK and jK . Considering the column-wise sorting of the *lower symmetric part* of (19), it is immediate to recognize that \mathcal{M}_{odd} targets the elements $\{1, 3, 5, 7, 16, 18, 20, 27, 29, 34\}$.

Thus, the assembly indices for both K and G are built by the following instructions, (see lines 26-42)

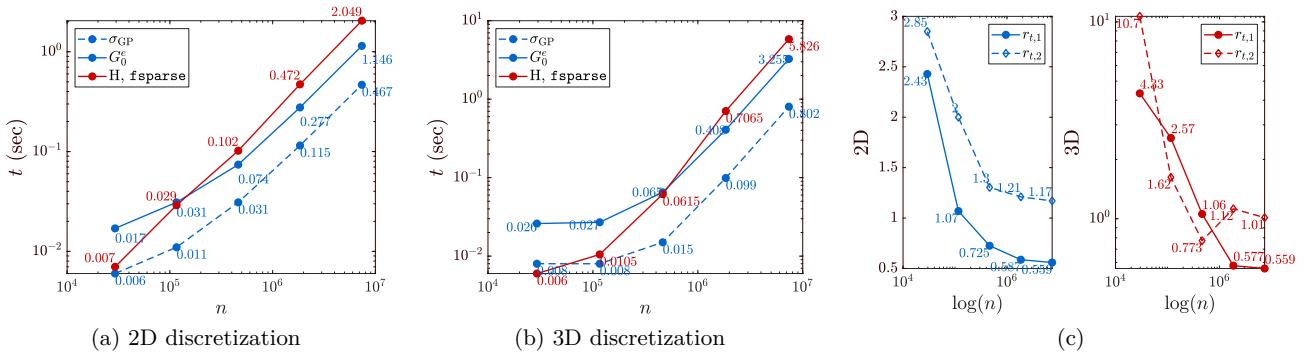


Fig. 2: Scaling of CPU time for the construction of the stress stiffness matrix G (a,b). The overall time is split between that for the stresses computation (σ_{GP}), for computing the compact representation Z of the elemental matrices (G_0^e), and that for assembling the global matrix ($H, \text{fsparse}$). In (c) we see the scaling of the ratios $r_{t,1} = \frac{\sigma_{GP} + G_0^e}{H, \text{fsparse}}$, measuring the efficiency of the elemental matrices setup, and $r_{t,2}$, comparing the overall time for setting up G with that for setting up K

```

[sI, sII]=deal([]); % Line 26
for j=1:8 % Line 27
    sI = cat(2, sI, j:8); % Line 28
    sII = cat(2, sII, repmat(j,1,8-j+1)); % Line 29
end % Line 30
[iK, jK] = deal(cMat(:, sI)', cMat(:, sII)'); % Line 31
Iar = sort([iK(:), jK(:)], 2, 'descend'); % Line 32
indM = [1, 3, 5, 7, 16, 18, 20, 27, 29, 34]; % Line 40
[iG, jG] = deal(iK(indM,:), jK(indM,:)); % Line 41
IkG = sort([iG(:), jG(:)], 2, 'descend'); % Line 42
    
```

Finally, the lower symmetric part of G is assembled by using `fsparse` (Engblom and Lukarski, 2016) (see lines 146-147)

```

G=fsparse(IkG(:,1)+1, IkG(:,2)+1, sG, [nDof, nDof])+
    fsparse(IkG(:,1), IkG(:,2), sG, [nDof, nDof]);
    
```

The same procedure can be extended to a 3D discretization with \mathcal{H}_8 trilinear elements. Equation 20 becomes $((i, k) = 1, \dots, 8)$

$$z_{ik} = \sigma_x a_k a_i + \sigma_y b_k b_i + \sigma_z c_k c_i + \tau_{xy} (b_k a_i + a_k b_i) + \tau_{xz} (a_k c_i + c_k a_i) + \tau_{yz} (b_k c_i + c_k b_i)$$

where $c_i = \partial_z N_i$ and the pattern of $G_{\{\mathcal{H}_8\}}^e$ is formally similar to that of (19). For the 3D case, computational cuts are much more substantial, as there are just 36 independent coefficients out of 576.

We refer to Figure 2 for considerations about the efficiency. Plots (a,b) show the scaling curves for the CPU time spent on computing the elemental stresses ($t[\sigma_{GP}]$) and the elemental geometric stiffness matrices $t[G_0^e]$. As n increases, the sum of these two times becomes smaller than the time spent on the G assembly operation ($t[H, \text{fsparse}]$). We notice that the assembly is a bit cheaper for the stress stiffness matrix than for the stiffness one, due to the larger sparsity of G (only $1/2$ of the $z_{ik} \neq 0$, whereas K_0^e is full).

Figure 2 (c) shows the trend of two coefficients measuring the efficiency of the operations for building the

global stress stiffness matrix G . $r_{t,1}$ is the ratio between $t[\sigma_{GP}] + t[G_0^e]$ (i.e. the overall time for computing the independent coefficients of the elemental stress stiffness matrices) and $t[H, \text{fsparse}]$. For small discretizations we have $r_{t,1} > 1$. This is reasonable because the assembly operation is extremely cheap and some operations for computing G_0^e (e.g. the short loop on Gauss knots) are not amortized by the efficiency of the vector products. However, as n increases $r_{t,1}$ drops as the computation of G_0^e takes advantage of the fully vectorized operations. $r_{t,2}$ is the ratio between the overall times for setting up G and that for K . Also this term decreases as the DOFs number n becomes larger, and for very large 2D discretizations the computation of G is about 17% in 2D, and only 1% in 3D, more expensive than computing K .

Therefore, the procedure we have described cuts the cost for setting up the buckling eigenvalue problem to the same as the one for setting up the linear analysis.

4.2 Sensitivity expressions

The \hat{x}_e -derivatives of the elemental matrices, needed for the expressions (9) and (10), are given by

$$\frac{\partial K^e}{\partial \hat{x}_e} = \frac{\partial E_K(\hat{x}_e)}{\partial \hat{x}_e} K_0^e, \quad \frac{\partial G^e}{\partial \hat{x}_e} = \frac{\partial E_G(\hat{x}_e)}{\partial \hat{x}_e} G_0^e \quad (23)$$

and the gradient of the compliance is computed as usual (Andreassen et al, 2011; Ferrari and Sigmund, 2020a), expressing the local product $\mathbf{u}_e^T K_0^e \mathbf{u}_e$ through the connectivity matrix (line 121).

Below we give details about how to take advantage of the compact representation introduced for G_0^e (i.e. $Z \in \mathbb{R}^{m \times 10}$) when expressing each term of (10).

\mathbf{p}_1	$(\varphi_1^2 + \varphi_2^2)$
\mathbf{p}_2	$(\varphi_1\varphi_3 + \varphi_2\varphi_4)$
\mathbf{p}_3	$(\varphi_1\varphi_5 + \varphi_2\varphi_6)$
\mathbf{p}_4	$(\varphi_1\varphi_7 + \varphi_2\varphi_8)$
\mathbf{p}_5	$(\varphi_3^2 + \varphi_4^2)$
\mathbf{p}_6	$(\varphi_3\varphi_5 + \varphi_4\varphi_6)$
\mathbf{p}_7	$(\varphi_3\varphi_7 + \varphi_4\varphi_8)$
\mathbf{p}_8	$(\varphi_5^2 + \varphi_6^2)$
\mathbf{p}_9	$(\varphi_5\varphi_7 + \varphi_6\varphi_8)$
\mathbf{p}_{10}	$(\varphi_7^2 + \varphi_8^2)$

Table 2: Mapping of the eigenvector components into the array \mathbf{p} used for writing the product $\varphi^T G_0^e \varphi \equiv \tilde{\mathbf{Z}} \odot \mathbf{p}$

Contribution 1. To express this at the element level we need to account for the structure of \mathbf{Z} . Writing out explicitly the double product we obtain

$$\begin{aligned} \varphi^T G_0^e \varphi &= (\varphi_1^2 + \varphi_2^2) z_{11} + (\varphi_3^2 + \varphi_4^2) z_{22} \\ &+ (\varphi_5^2 + \varphi_6^2) z_{33} + (\varphi_7^2 + \varphi_8^2) z_{44} \\ &+ 2(\varphi_1\varphi_3 + \varphi_2\varphi_4) z_{21} + 2(\varphi_1\varphi_5 + \varphi_2\varphi_6) z_{31} \\ &+ 2(\varphi_1\varphi_7 + \varphi_2\varphi_8) z_{41} + 2(\varphi_3\varphi_5 + \varphi_4\varphi_6) z_{32} \\ &+ 2(\varphi_3\varphi_7 + \varphi_4\varphi_8) z_{42} + 2(\varphi_5\varphi_7 + \varphi_6\varphi_8) z_{43} \end{aligned} \quad (24)$$

where we have exploited the symmetry of z_{ij} and we have set $\varphi = \varphi_e$ for simplicity. The same result of (24) can be obtained with the Hadamard product $\tilde{\mathbf{Z}} \odot \mathbf{p}$, where $\mathbf{p} \in \mathbb{R}^{10 \times m}$ collects the components of φ as shown in Table 2, for all the elements. A quick glance at the subscripts in Table 2 reveals that the array \mathbf{p} can be built by using the indices $i\mathbf{G}$ and $j\mathbf{G}$. Indeed, we recognize $\mathbf{p}_i = \varphi_{\mathcal{M}_{\text{odd}}(i,2)} \varphi_{\mathcal{M}_{\text{odd}}(i,1)} + \varphi_{\mathcal{M}_{\text{even}}(i,2)} \varphi_{\mathcal{M}_{\text{even}}(i,1)}$; thus we formally express $\mathbf{p} = \varphi(\mathcal{M})$, where $\mathcal{M} \in \mathbb{N}^{10 \times m}$.

To have consistency with (24) the elements on columns $\{2, 3, 4, 6, 7, 9\}$ of the array \mathbf{Z} must be doubled, obtaining $\tilde{\mathbf{Z}}$. This first contribution could be computed by the following operations

```
t2ind=[2,3,4,6,7,9];           % defined on Line 40
a1=reshape(IkG(:,2),10,nE1)';   % defined on Line 43
a2=reshape(IkG(:,1),10,nE1)';   % defined on Line 43
dkeG=dsG.*Z;                   % x-derivative of G
dkeG(:,t2ind)=2*dkeG(:,t2ind); % 2x t2ind columns
for j=1:nEig
    t=phi(:,j);
    vC=t(a1).*t(a2)+t(a1+1).*t(a2+1);
    phiDGphi(:,j)=sum(dkeG.*vC,2);
end
```

similar to those in the code of Appendix C.

Contribution 2 The double product $\varphi^T (\partial_e K) \varphi$ can be computed at the element level as done for $\partial_e c$, upon replacing $\partial_e E_K(x_e)$ by $\partial_e E_G(x_e)$ and \mathbf{u} by φ .

Contribution 3 The derivative of the non-dimensional elemental stress stiffness matrix G_0^e with respect to each component u_i of the displacement vector \mathbf{u} reads (see

Equation 17)

$$\begin{aligned} \frac{\partial G_0^e}{\partial u_i}(\mathbf{u}) &= \frac{\partial}{\partial u_i} \int_{\Omega_e} B_1^T \left(I_2 \otimes \frac{\partial \boldsymbol{\sigma}^e}{\partial u_i} \right) B_1 d\Omega_e \\ &= \int_{\Omega_e} B_1^T \left(I_2 \otimes C B_0 \frac{\partial \mathbf{u}_e}{\partial u_i} \right) B_1 d\Omega_e \\ &= \int_{\Omega_e} B_1^T (I_2 \otimes C B_0 \delta_{ie}) B_1 d\Omega_e \end{aligned} \quad (25)$$

where $\delta_{ie} = 1$ if u_i belongs to the displacements \mathbf{u}_e on element e , and $\delta_{ie} = 0$ otherwise.

Since (25) is independent of $\hat{\mathbf{x}}$, a simple way to obtain the gradient $\nabla_{\mathbf{u}} G_0^e$ is to pre-compute the operator $\nabla_{\mathbf{u}} \mathbf{Z} \in \mathbb{R}^{10 \times 8}$. Following the same reduced storage format of \mathbf{Z} , the i -th column of $\nabla_{\mathbf{u}} \mathbf{Z}$ contains the 10 independent coefficients of the stress stiffness matrix corresponding to the displacement vector $\mathbf{u} \in \mathbb{R}^{8 \times 1}$, $u_i = 1$, $u_{j \neq i} = 0$; namely,

$$\nabla_{\mathbf{u}} \mathbf{Z} = [G_0^e(u_1 = 1), G_0^e(u_2 = 1), \dots, G_0^e(u_8 = 1)] \quad (26)$$

Equation 26, called `dZdu` in the code, is computed between lines 44-58, using the compact definitions of B_0 and B_1 given in Appendix A. Then, each adjoint load can be computed by expressing the following double product

$$\varphi_i^T (\nabla_{\mathbf{u}} G) \varphi_i = (\nabla_{\mathbf{u}} \tilde{\mathbf{Z}}) \odot \mathbf{p} \quad (27)$$

as described for Contribution ①, where \mathbf{p} is as in Table 2 and $\nabla_{\mathbf{u}} \tilde{\mathbf{Z}}$ is obtained from $\nabla_{\mathbf{u}} \mathbf{Z}$ by doubling the elements of columns $\{2, 3, 4, 6, 7, 9\}$. Once the adjoint problem has been solved for \mathbf{w}_i , the computation of the last sensitivity term only requires another application of step ②, with \mathbf{u} and \mathbf{w}_i as left and right vectors, respectively.

Sensitivity calculations are implemented in the code of Appendix C between lines 156-180. However, in order to reduce looping and avoid repeated calculations, the operations are grouped in a slightly different way. Within a single loop, we extract each of the `nEig` modes, compute contribution ② (Line 160-161), build the array \mathbf{p} only once (Line 163), and use this for computing contribution ① (Line 164) and the adjoint loads (Line 168). Then, the adjoint problem is solved simultaneously for all the right hand sides and contribution ③ is computed between lines 173-177. Finally, the sensitivities of the BLFs-related quantities μ_i are given by Line 179.

4.3 Solution of state and adjoint equations

If buckling is among the optimization criteria, two linear systems and an eigenvalue problem have to be solved

at each re-design step. It is outside the scope of the present work to discuss how to perform this with highly efficient methods, and we leave this extension to the interested users. Here we resort to built-in Matlab functions, whose efficiency is satisfactory for medium-scale 2D problems.

The stiffness matrix K is decomposed by the Cholesky factorization, using the `decomposition` Matlab function. The factor `dK` is stored (Line 119) and used for solving both the linear equilibrium equations (Line 120) and the adjoint problem (Line 173). `dK` is useful also when calling the `eigs` function for solving the eigenvalue problem (7). This is done by the following instructions (see lines 151-152)

```
matFun = @(v) dK\Kgeo(free,free)*v;
[eivecs,D]=eigs(matFun,length(free),nEig+4,'sa');
```

where the map $\mathbf{v} \mapsto K^{-1}G\mathbf{v}$, repeatedly performed by the iterative Krylov method underlying `eigs` (Lehoucq and Sorensen, 1996; Stewart, 2002), is explicitly given by the function `matFun`. This spares the re-factorization of K within `eigs`, and we have observed a cut of about 10-15% of the CPU time, compared to the case where `matFun` is not provided. When the eigenvalues get close, Krylov based method may loose accuracy on the “last” computed eigenpairs (Wendland, 2018). Therefore, we heuristically set the number of computed eigenpairs to `nEig+4`, to retain good accuracy on the `nEig` used for running the optimization. The argument `'sa'` selects the smallest algebraic (i.e. “most negative”) eigenvalues $D(i)$. Thus, $-D(i)$ correspond to the μ_i of our formulation and, since $\mu_i = 1/\lambda_i$, to the smallest positive BLFs. Within our assumption of having a load with *fixed* direction it is physically meaningful to account for positive eigenvalues only. However, the code of Appendix C could be extended to handle more general loading conditions by properly redefining the eigenvalue equation and the combination of the sensitivity terms in (10) (see e.g., Lund (2009)).

Finally, a difference with respect to `top99neo` is that we need to recover the full K and G matrices (lines 118, 149) in order to get correct eigenpairs from `eigs`. However, the cost of this operation is minor, and essentially identical to the symmetrization operation in `top88` (Andreassen et al, 2011).

5 Examples

We present two examples, demonstrating the capabilities of the code provided in Appendix C. We set $E_0 = 1$, $E_{\min} = 10^{-6}$, $\nu = 0.3$ and we adopt the interpolations (3) for all the following problems. The tests have been run on a laptop equipped with an Intel(R) Core(TM)

i7-5500U@2.40GHz CPU, 15GB of RAM and Matlab 2018b running in serial mode under Ubuntu 18.04.

5.1 BLF maximization of a compressed column

We consider the cantilever of Figure 3 (a) discretized by $\Omega_h = 480 \times 240$ elements. The load is spread over the length $b/L_y = 1/15$ at the top and has total magnitude $|q| = 1 \cdot 10^{-3}$. The rectangular area of 10×20 elements near the load constitutes \mathcal{P}_1 while $\mathcal{P}_0 = \emptyset$. The boundary conditions and passive regions are implemented by default in the code at lines 64-69, and we remark that the uniform force density $|F_i| = 0.625$ is applied on the interior nodes of b , whereas $|F_i| = 0.3125$ for the two border nodes, for consistency.

We obtain the minimum volume design starting from the fully solid domain ($\mathbf{x} = \mathbf{1}_m$) and for the maximum allowed compliance $\bar{c} = 2.5c_{x=1}$, where $c_{x=1}$ is the initial compliance. Explicitly, we solve

$$\begin{cases} \min_{\mathbf{x} \in [0,1]^m} f(\hat{\mathbf{x}}) \\ \text{s.t. } g_c(\hat{\mathbf{x}}) = \mathbf{F}^T \mathbf{u}(\hat{\mathbf{x}}) / \bar{c} - 1 \leq 0 \end{cases} \quad (28)$$

and we set $p = 3$, fixed throughout the optimization and $r_{\min} = 4$ elements for the density filter. The projection parameters are $\eta = 0.5$, $\beta = 2$ and the continuation scheme on β follows the rule `cntBeta={150,12,25,2}`. The code in Appendix C is called as follows

```
topBuck250(480,240,3,4,2,'N',0.5,2,[0.1,0.7,1.2],
300,2,penalG,nEig,pAgg,{'V','C'},2.5)
```

where `penalG`, `nEig`, `pAgg` can take any value, because all the buckling-related operations are skipped.

The optimized design, shown in Figure 3 (a), has a volume fraction $f^* \approx 0.24$ and meets the compliance requirement ($g_c^* \approx -1 \cdot 10^{-7}$, thus the constraint is active), but is clearly very prone to lateral buckling. Indeed, we have $\lambda_1 \approx 0.75$, which means that this design would buckle under the applied load magnitude.

Therefore, we reinforce the design by solving the BLF maximization problem (13) with volume fraction and compliance upper bounds $\bar{f} = 0.25$ and $\bar{c} = 2.5c^*$, respectively, where $c^* = 8.57 \cdot 10^{-6}$ is the compliance attained by the minimum volume design. The lowest 12 BLFs are aggregated in the KS function, and the aggregation parameter is set to $\rho = 160$, constant throughout the process. Such a high value of the aggregation parameter is no harm to the numerical stability of the KS function (8) (Raspanti et al, 2000), and is needed to keep a good approximation, especially for the aggregation of constraints. The penalization and filter parameters are chosen as before, but now we adopt $\beta = 6$, and the continuation on this parameter is changed to

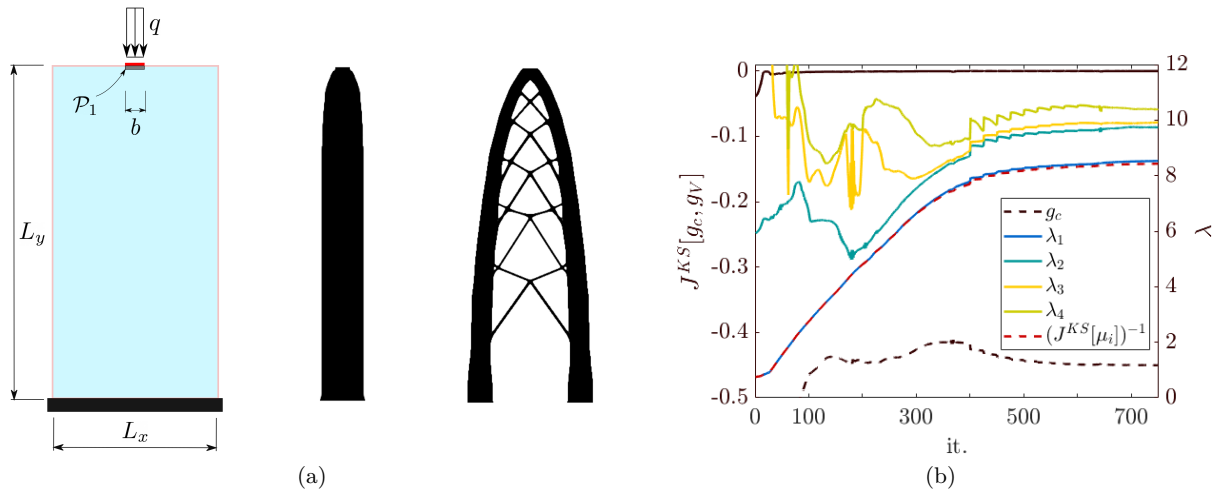


Fig. 3: (a) Geometrical sketch for the compressed column example (leftmost), minimum volume design (center) and buckling reinforced design (rightmost). The minimum volume design has a volume fraction $f \approx 0.24$, compliance $c^* = 8.57 \cdot 10^{-6}$ and BLF $\lambda_1 = 0.75$. The buckling design has volume fraction $f = 0.25$ (the volume constraint is tight), compliance $\approx 1.4c^*$ and $\lambda_1 = 8.53$. (b) shows the evolution of the aggregated constraint (essentially coincident with g_V) and of the compliance constraint g_c , plotted against the left axis, and of the lowest four BLFs and the reciprocal of the KS function, plotted against the right axis

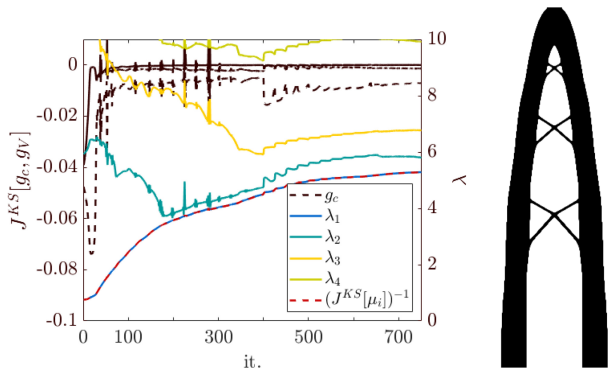


Fig. 4: Buckling-reinforced design corresponding to the compliance upper bound $\bar{c} = 1.05c^*$ and volume fraction $\bar{f} = 0.25$ (see Figure 3 for comparison). The final value attained by the fundamental BLF is $\lambda_1 = 5.28$. The compliance constraint (black dashed curve) now becomes closer to the volume one (black dash-dotted curve), and contributes up to 40% to the KS aggregated constraint value (black continuous curve)

`betaCnt={400,24,25,2}`. In this context, a higher β parameter was chosen as a simple way to attenuate the artificial buckling mode phenomenon (Neves et al, 2002). Further analyses on this topic, and the implementation of more advanced remedies are left to the interested users.

Assuming that the minimum volume design has been saved in the file 'IG.mat', we call

```
topBuck250(480,240,3,4,2,'N',0.5,2,[0.1,0.7,1.2],
750,2,3,12,200,{'B','C','V'},[2.5,0.25])
```

The final design, shown in Figure 3 (a), carries over 10 times more load before buckling than the initial one

(λ_1 increases from 0.75 to 8.53), and this comes at a slight increase of volume ($\approx 4\%$), and a stiffness reduction of about 30%; however, the compliance constraint never becomes active. Figure 3 (b) shows the evolution of the aggregated constraint, of the (inverse) objective and of the lowest 4 BLFs. Due to the rather high ρ value, the lower bound given by $(J_0^{KS})^{-1}$ is a good approximation to λ_1 in the whole optimization history.

Figure 4 shows the design obtained when reducing the maximum allowed compliance to $\bar{c} = 1.05c^*$. The compliance constraint now becomes much more important, and contributes 30-45% to the overall constraint sensitivity, throughout the optimization. Because of the tightened compliance constraint allowing less freedom (Gao and Ma, 2015; Ferrari and Sigmund, 2019), the fundamental BLF now attains only a lower value of $\lambda_1 = 5.28$.

Figure 4 and other tests we have performed indicate that the simple OC scheme implemented in `ocUpdate` can cope with the situation where both constraints become very close. However, oscillations in the convergence history may happen as the two constraints become (almost) active, and this may hamper the robustness of the update scheme, especially if the volume-preserving projection is selected (`ft=3`), and high β values are used. In such cases, users are encouraged to shift to more robust optimizers, such as the MMA (see Appendix B).

Concerning the computational cost, the whole optimization process (750 re-design steps) takes about 12,900s ($\approx 17.5s$ per iteration). Of this time, 85.4% ($\approx 11,000s$) is spent solving the eigenvalue problem,

5.8% ($\approx 750s$) solving the linear equilibrium equations and 1.1% ($\approx 146.5s$) solving the adjoint problem. All the other operations are very cheap and, in particular, the overall time fraction spent on the construction of the stress stiffness matrix is 0.3% ($\approx 48s$) and that for the sensitivity analysis is 5% ($\approx 665.2s$). The overall time spent on the `ocUpdate` (see Appendix B) for updating the design variables is 0.6% ($\approx 78s$).

The time spent on the state and adjoint analyses, representing the vast majority of the overall one, can be largely cut by using efficient multi-level solvers for both linear and eigenvalue equations, and this would make buckling optimization with the `topBuck250` essentially as efficient as multiple-load compliance optimization (Ferrari and Sigmund, 2020b).

5.2 Wall-reinforcement problem

Figure 5 shows a wall with an opening (represented by the passive void region \mathcal{P}_0). The outer frame of the wall and of the opening are both surrounded by a solid frame (\mathcal{P}_1) with thickness $t = L/40$, clamped at the base. The outer frame alone represents a suitable load transfer path for the applied load q , but would result in a structure that is too compliant.

Therefore, the goal is to find the minimum weight configuration of reinforcement material in the active domain \mathcal{A} , starting from the full solid design (i.e. $\mathbf{x} = 1$ on \mathcal{A} , corresponding to a volume fraction of ≈ 0.76 of the overall domain $\mathcal{A} \cup \mathcal{P}_1 \cup \mathcal{P}_0$). To do this, we refer to problem (14), where \bar{c} is again set to 2.5 times the compliance of the full design, and the BLF is kept above the value $\underline{\lambda}$, by applying the constraints g_c and g_λ of (15).

We set $L = 1$, $\Omega_h = 320 \times 320$ and the load, uniformly distributed over the whole left edge, has total magnitude $|q| = 10^{-2}$. To implement this example we only need to replace lines 64-70 with the following

```
fixedNodes=nodeNrs(end,[1:9,120:128,257:265,313:321])
fixed=[2*fixedNodes,2*fixedNodes-1];
lcDof=2*nodeNrs(1:end,1)-1;
modF=1e-2/Ly/(length(lcDof)-1);
F=fsparse(lcDof,1,modF,[nDof,1]);
[F(lcDof(1)),F(lcDof(end))]=deal(F(lcDof(1))/2,F(lcDof(end))/2);
a1=e1Nrs(1:nely/40,:);
a2=e1Nrs(:,[1:nely/40,end-nely/40+1:end]);
a3=e1Nrs(2*nely/5:end,2*nely/5:end-nely/5);
a4=e1Nrs(2*nely/5-nely/40:end,2*nely/5-nely/40:2*nely/5-1);
a5=e1Nrs(2*nely/5-nely/40:end,end-nely/5+1:end-nely/5+nely/40);
a6=e1Nrs(2*nely/5-nely/40:2*nely/5-1,2*nely/5:end-nely/5);
[pass, pasV]=deal(unique([a1(:);a2(:);a4(:);a5(:);a6(:)]), a3(:));
```

The other parameters for the optimization are chosen as follows: p_K and p_G are increased from 3 to 6, both according to the continuation scheme $\{25, 6, 25, 0.25\}$, $\eta = 0.5$ and β is increased from 2 to 12 according to the continuation scheme $\text{betaIncrease}=\{325, 12, 25, 2\}$. The density filter radius is $r_{\min} = 3$ and the lowest 12 BLFs are aggregated in the KS function, with $\rho = 160$.

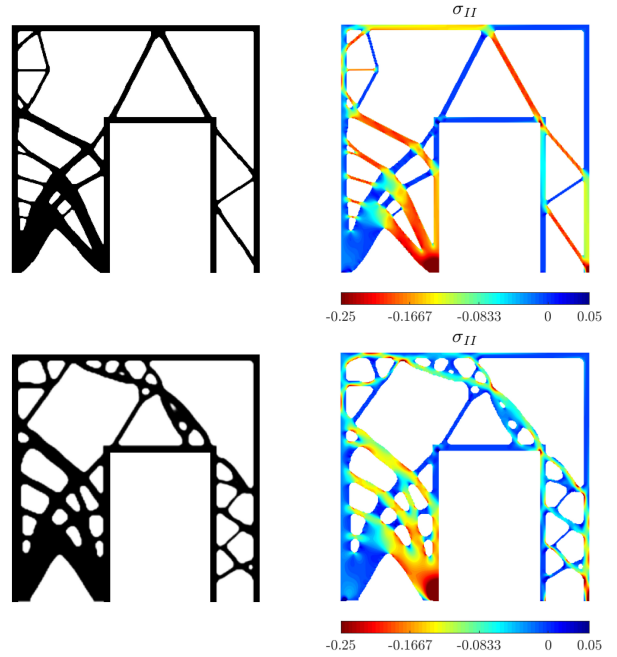
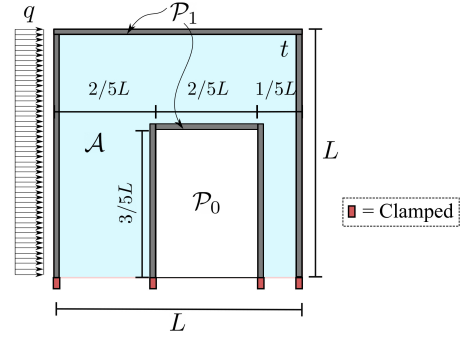


Fig. 5: Geometrical setup for the wall reinforcement problem (top), minimum volume design obtained with the compliance constraint alone (middle row) and with a lower bound $\underline{\lambda} = 1.05$ on the BLF (bottom row). Plots on the right column show the distribution of the minimum principal stresses σ_{II}

The middle row of Figure 5 shows the optimized design obtained by calling the code in Appendix C as

```
topBuck250(320,320,3,3,2,'N',0.5,2,[0.1,0.7,1.2],
500,1,penalG,nEig,pAgg,{'V','C'},2.5)
```

thus, without the buckling constraint ($\underline{\lambda} = 0$). For this design, the compliance constraint is tight ($g_c^* \approx 10^{-9}$) and the volume fraction attains the value $f^* = 0.245$.

The reinforcement material is concentrated in the lower left part of the structure, assuming a configuration that vaguely resembles that of an optimized cantilever for a tip load. Elsewhere, the reinforcement material is organized in slender bars. This design is clearly not effective against buckling, as can be seen from the distribution of the minimum principal stresses (σ_{II}) in the rightmost plot of Figure 5. From this plot we ac-

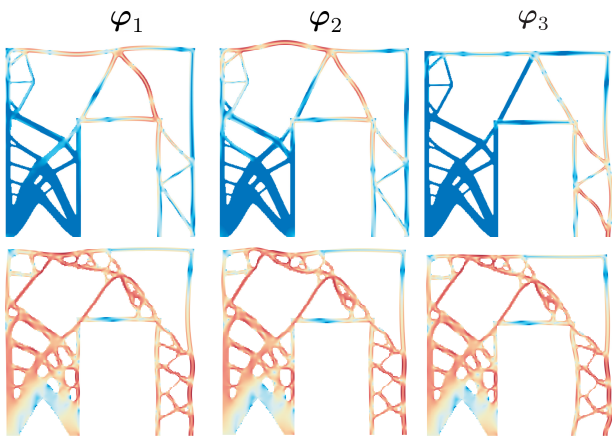


Fig. 6: The lowest three buckling modes (φ_i) for the wall reinforced design, obtained without (top row) and with (bottom row) the buckling constraint. The colorscale (blue to red) follows the logarithm of the strain energy density (low to high)

knowledge that some thin bars are subject to relatively high compression, and from Figure 6 we see that they are indeed undergoing localized buckling. The fundamental BLF is $\lambda_1 = 3.15$ for the initial, solid structure and $\lambda_1 = 0.15$ for the minimum volume design. Therefore, this latter is of little practical use.

To obtain a more realistic design, we solve again the optimization problem imposing the lower bound $\underline{\lambda} = 1.05$ to the BLF, calling the routine by

```
topBuck250(320,320,3,3,2,'N',0.5,2,[0.1,0.7,1.2],
500,1,3,12,160,{'V','C','B'},[2.5,1.05])
```

and the continuation on p_G is identical to that on p_K .

We obtain the design shown in the bottom row of Figure 5, having a volume fraction $f^* = 0.33$ and fulfilling both constraints. The minimum principal stress (σ_{II}) plot shows that the thinnest bars are now subjected to tension only, whereas compressed parts have a more organic, frame-like configuration. By comparing the distribution of the compressive stresses with the lowest three buckling modes depicted in Figure 6, we observe that now buckling is triggered by a deformation in the outer frame, and this endows the structure with a much better overall behavior.

6 Conclusions

We have presented a compact Matlab implementation that allows for solution of buckling TO problems on a laptop, up to a scale that is limited only by the solution of the eigenvalue problem, which is now absorbing the vast majority of the CPU time. The setup of the stress stiffness matrix and the sensitivity analysis of the buckling load factor are made very cheap by rethinking their

standard construction and using a fully vectorized implementation. Otherwise, these operations alone would make solution of the problem in Matlab very slow.

The code provided in Appendix C can be immediately used to solve problems for the maximization of the buckling load factor with compliance and volume constraints, and for the minimization of volume with buckling and compliance constraints. The basic TO problems of volume constrained compliance minimization and *vice versa* can also be run avoiding all the buckling related operations; thus obtaining a code with the same efficiency as `top99neo`. However, the code can easily be extended to more general problems involving these three criteria, and to implement more advanced formulations and solution methods. As an example, methods to deal with the artificial modes phenomenon, here overlooked, can easily be implemented. Also, preconditioned eigensolvers (Dunning et al, 2016) and multilevel methods (Ferrari and Sigmund, 2020b) are easy to implement in the present code, to alleviate the burden of the eigenvalue solution. Finally, we point out that other problems that involve element-wise operations, such as non-linear elasticity or orientation dependent material properties, may be effectively reformulated with a strategy similar to what is described here.

Therefore, we believe that the present code can be a helpful contribution to researchers and practitioners who aim at solving TO problems with buckling criteria in Matlab, and provide food for thought to anyone seeking efficient implementations of potentially time consuming problems in FE analysis and TO.

Acknowledgements The authors FF and JKG acknowledge the support of the National Aeronautics and Space Administration (NASA) under Grant No. 80NSSC18K0428. The opinions, findings, and conclusions or recommendations expressed in this paper are those of the authors and do not necessarily reflect the views of NASA. OS is supported by the Villum Fonden through the Villum Investigator Project “InnoTop”.

Reproducibility of results Matlab code is listed in the Appendix and available at www.topopt.dtu.dk. The `stenglib` package, containing the `fsparse` function, is available for download at <https://github.com/stefanengblom/stenglib>.

References

- Andreassen E, Clausen A, Schevenels M, Lazarov BS, Sigmund O (2011) Efficient topology optimization in matlab using 88 lines of code. *Structural and Multidisciplinary Optimization* 43(1):1–16, DOI 10.1007/s00158-010-0594-7
- Bathe KJ (1982) *Finite Element procedures in engineering analysis*, 1st edn
- Bendsøe MP, Sigmund O (2004) *Topology Optimization: Theory, Methods and Applications*. Springer

- de Borst R, Crisfield MA, Remmers JJC, Verhoosel CV (2012) Non-Linear Finite Element Analysis of Solids and Structures, second edition edn. John Wiley & Sons
- Bourdin B (2001) Filters in topology optimization. *International Journal for Numerical Methods in Engineering* 50(9):2143–2158, DOI 10.1002/nme.116
- Brent R (1973) Algorithms for Minimization without Derivatives. Prentice Hall
- Bruns TE, Tortorelli DA (2001) Topology optimization of non-linear elastic structures and compliant mechanisms. *Computer Methods in Applied Mechanics and Engineering* 190(26):3443 – 3459, DOI [http://dx.doi.org/10.1016/S0045-7825\(00\)00278-4](http://dx.doi.org/10.1016/S0045-7825(00)00278-4), URL <http://www.sciencedirect.com/science/article/pii/S0045782500002784>
- Bruyneel M, Colson B, Remouchamps A (2008) Discussion on some convergence problems in buckling optimisation. *Structural and Multidisciplinary Optimization* 35(2):181–186
- Crisfield MA (1991) Nonlinear finite element analysis of solid and structures, vol I. Wiley
- Dunning PD, Ovtchinnikov E, Scott J, Kim A (2016) Level-set topology optimization with many linear buckling constraints using an efficient and robust eigensolver. *International Journal for Numerical Methods in Engineering*
- Engblom S, Lukarski D (2016) Fast matlab compatible sparse assembly on multicore computers. *Parallel Computing* 56:1–17
- Ferrari F, Sigmund O (2019) Revisiting topology optimization with buckling constraints. *Structural and Multidisciplinary Optimization* 59(5):1401–1415, DOI 10.1007/s00158-019-02253-3
- Ferrari F, Sigmund O (2020a) A new generation 99 line matlab code for compliance topology optimization and its extension to 3d. *Structural and Multidisciplinary Optimization* 62:2211–2228
- Ferrari F, Sigmund O (2020b) Towards solving large-scale topology optimization problems with buckling constraints at the cost of linear analyses. *Computer Methods in Applied Mechanics and Engineering* 363:112,911, DOI <https://doi.org/10.1016/j.cma.2020.112911>
- Gao X, Ma H (2015) Topology optimization of continuum structures under buckling constraints. *Computers & Structures* 157:142–152
- Gravesen J, Evgrafov A, Nguyen DM (2011) On the sensitivities of multiple eigenvalues. *Structural and Multidisciplinary Optimization* 44(4):583–587
- Groenwold AA, Etman LFP (2008) On the equivalence of optimality criterion and sequential approximate optimization methods in the classical topology layout problem. *Internal Journal for Numerical Methods in Engineering* 73:297–316
- Guest JK, Prévost JH, Belytschko T (2004) Achieving minimum length scale in topology optimization using nodal design variables and projection functions. *International Journal for Numerical Methods in Engineering* 61(2):238–254, DOI 10.1002/nme.1064
- Guest JK, Asadpoure A, a SH (2011) Eliminating beta continuation from heaviside projection and density filter algorithms. *Structural and Multidisciplinary Optimization* 44(4):443–453
- Kennedy GJ, Hicken JE (2015) Improved constraint-aggregation methods. *Computer Methods in Applied Mechanics and Engineering* 289(Supplement C):332 – 354
- Kreisselmeier G, Steinhauser R (1979) Systematic control design by optimizing a vector performance index. *IFAC Proceedings Volumes* 12(7):113 – 117, iFAC Symposium on computer Aided Design of Control Systems, Zurich, Switzerland, 29-31 August
- Lehoucq R, Sorensen DC (1996) Deflation techniques for an implicitly re-started arnoldi iteration. *SIAM J Matrix Anal Appl* 17:789–821
- Lund E (2009) Buckling topology optimization of laminated multi-material composite shell structures. *Composite Structures* 91(2):158–167
- Neves MM, Sigmund O, Bendsøe MP (2002) Topology optimization of periodic microstructures with a penalization of highly localized buckling modes. *International Journal for Numerical Methods in Engineering* 54(6):809–834
- Raspanti CG, Bandoni JA, Biegler LT (2000) New strategies for flexibility analysis and desing under uncertainties. *Computers & Chemical Engineering* 24:2193–2209
- Rodrigues HC, Guedes JM, Bendsøe MP (1995) Necessary conditions for optimal design of structures with a nonsmooth eigenvalue based criterion. *Structural Optimization* 9:52–56
- Seyranian AP, Lund E, Olhoff N (1994) Multiple eigenvalues in structural optimization problems. *Structural optimization* 8(4):207–227
- Sigmund O (2001) A 99 line topology optimization code written in Matlab. *Structural and Multidisciplinary Optimization* 21(2):120–127, DOI 10.1007/s001580050176
- Sigmund O (2007) Morphology-based black and white filters for topology optimization. *Structural and Multidisciplinary Optimization* 33(4):401–424
- Stewart G (2002) A Krylov-Schur algorithm for large eigenproblems. *SIAM Journal on Matrix Analysis and Applications* 23(3):601–614
- Svanberg K (1987) The method of moving asymptotes - A new method for structural optimization. *International Journal for Numerical Methods in Engineering* 24(2):359–373
- Svanberg K (2002) A class of globally convergent optimization methods based on conservative convex separable approximations. *SIAM Journal on Optimization* 12(2):555–573, DOI 10.1137/S1052623499362822
- Svanberg K (2007) MMA and GCMMA—two methods for nonlinear optimization, available for download at <https://people.kth.se/~krille/mmagmma.pdf>
- Wahlbin LB (1995) Superconvergence in galerkin finite element methods. In: *Lecture Notes in Mathematics, Lecture Notes in Mathematics*, vol 1605, Springer, Berlin, Heidelberg
- Wang F, Lazarov B, Sigmund O (2011) On projection methods, convergence and robust formulations in topology optimization. *Structural and Multidisciplinary Optimization* 43(6):767–784
- Wendland H (2018) *Numerical linear algebra: An introduction*. Cambridge texts in applied mathematics, Cambridge University Press
- Wrenn G (1989) An indirect method for numerical optimization using the Kreisselmeir–Steinhauser function. Tech. rep., URL <https://books.google.it/books?id=LjsCAAAIAAJ>
- Xia L, Breitkopf P (2015) Design of materials using topology optimization and energy-based homogenization approach in matlab. *Structural and Multidisciplinary Optimization* 52(6):1229–1241, DOI 10.1007/s00158-015-1294-0
- Yago D, Cante J, Lloberas-Valls O, Oliver J (2021) Topology optimization using the unsmooth variational topology optimization (unvartop) method: an educational implementation in matlab. *Structural and Multidisciplinary Optimization* 63:955–981
- Zienkiewicz O, Taylor R (2005) *The finite element method for solid and structural mechanics*, 6th edn. Elsevier

A Notes

Let $X^e = [x_i^e, y_i^e]_{i=1}^k$ be the array collecting the coordinates of a k -noded element and $N(\xi, \zeta) = [N_1(\xi, \zeta), N_2(\xi, \zeta), \dots, N_k(\xi, \zeta)]$ be the array collecting the shape functions, where (ξ, ζ) are the logical coordinates (Bathe, 1982). The (x, y) -gradient of the shape functions is computed as $\nabla_{(x,y)}N = J^{-1}\nabla_{(\xi,\zeta)}N$, where the (ξ, ζ) -gradient and Jacobian are

$$\begin{aligned} \nabla_{(\xi,\zeta)}N &= \begin{bmatrix} \partial_\xi N_1, \dots, \partial_\xi N_k \\ \partial_\zeta N_1, \dots, \partial_\zeta N_k \end{bmatrix} \\ J(\xi, \eta) &= \begin{bmatrix} \sum_k \partial_\xi N_k x_k & \sum_k \partial_\xi N_k y_k \\ \sum_k \partial_\zeta N_k x_k & \sum_k \partial_\zeta N_k y_k \end{bmatrix} = \nabla_{(\xi,\zeta)}N X^e \end{aligned} \quad (29)$$

The discretized deformation gradient (B_1) and strain-displacement operator (B_0) are then recovered as

$$\begin{aligned} B_1 &= \begin{bmatrix} \nabla_{(x,y)}N \otimes [1, 0]^T \\ \nabla_{(x,y)}N \otimes [0, 1]^T \end{bmatrix} \\ B_0 &= L(\nabla_{(x,y)}N \otimes I_2) \end{aligned} \quad (30)$$

where L is the placement matrix (here shown for a Q_4 element)

$$L = \begin{bmatrix} 1 & 0 & 0 & 0 \\ 0 & 0 & 0 & 1 \\ 0 & 1 & 1 & 0 \end{bmatrix}$$

and I_2 is the identity matrix of order 2.

The operations above have a remarkably compact implementation in the code of Appendix C, for the particular case of a Q_4 element (see lines extracted below).

```
lMat=zeros(3,4);lMat(1,1)=1;lMat(2,4)=1;lMat(3,2:3)
=1;
dN=@(xi,zi)0.25*[zi-1,1-zi,1+zi,-1-zi;xi-1,-1-xi,1+
xi,1-xi];
gradN=(dN(xi,zi)*xe)/dN(xi,zi)
B0=@(gradN) lMat*kron(gradN,eye(2))
B1=[kron(gradN,[1,0]);kron(gradN,[0,1])]
```

The instructions above could be further simplified, since we are considering a uniform discretization (i.e. J is constant). However, the current definition is general enough to be easily extended to higher order elements by only modifying the definition of `dN`.

B Details on the re-design rule and on the KS aggregation function

Let us have the two sets of functions $\{g_{0(i)}(\mathbf{x})\}_{i=1,\dots,q}$ and $\{g_j(\mathbf{x})\}_{j=1,\dots,s}$ and the following optimization problem

$$\begin{cases} \min_{\mathbf{x} \in [0,1]^m} \max_{i=1,\dots,q} g_{0(i)}(\mathbf{x}) \\ \text{s.t. } g_j(\mathbf{x}) \leq 0, & j = 1, \dots, s \end{cases} \quad (31)$$

We replace $J_0^{KS}(\mathbf{x}) := J^{KS}[g_{0(i)}(\mathbf{x})]$ to the ‘‘max’’ operator in the objective, and $J_1^{KS}(\mathbf{x}) := J^{KS}[g_j(\mathbf{x})]$ to the set of constraints, obtaining the single objective, single constraint problem

$$\begin{cases} \min_{\mathbf{x} \in [0,1]^m} J_0^{KS}(\mathbf{x}) \\ \text{s.t. } J_1^{KS}(\mathbf{x}) \leq 0 \end{cases} \quad (32)$$

which is analogous to (13). At the current design point ($\mathbf{x}_k = \boldsymbol{\xi}$) the objective and constraint functions are expanded in terms of intervening variables $y_e(x_e)$, $e = 1, \dots, m$, each selected such to build a convex approximation. Choosing an MMA-like form for the intervening variables (Svanberg, 1987), the objective ($i = 0$) and constraint ($i = 1$) are expanded as

$$\begin{aligned} J_i^{KS}(\mathbf{x}) &\approx J_i^{KS}(\boldsymbol{\xi}) + \sum_{e=1}^m \left[(U_e - \xi_e)^2 p_e^i(\boldsymbol{\xi}) \left(\frac{1}{U_e - x_e} - \frac{1}{U_e - \xi_e} \right) - (\xi_e - L_e)^2 q_e^i(\boldsymbol{\xi}) \left(\frac{1}{x_e - L_e} - \frac{1}{\xi_e - L_e} \right) \right] \\ &\underbrace{J_i^{KS}(\boldsymbol{\xi}) - \sum_{e=1}^m \left[(U_e - \xi_e)^2 p_e^i(\boldsymbol{\xi}) - (\xi_e - L_e)^2 q_e^i(\boldsymbol{\xi}) \right]}_{\widehat{J}_i^{KS}(\boldsymbol{\xi})} + \sum_{e=1}^m \left[\frac{(U_e - \xi_e)^2 p_e^i(\boldsymbol{\xi})}{U_e - x_e} - \frac{(\xi_e - L_e)^2 q_e^i(\boldsymbol{\xi})}{x_e - L_e} \right] \\ &= \widehat{J}_i^{KS}(\boldsymbol{\xi}) + \sum_{e=1}^m \left[\frac{(U_e - \xi_e)^2 p_e^i(\boldsymbol{\xi})}{U_e - x_e} - \frac{(\xi_e - L_e)^2 q_e^i(\boldsymbol{\xi})}{x_e - L_e} \right] \end{aligned} \quad (33)$$

where $p_e^i(\boldsymbol{\xi}) = \max\{\partial_e J_i^{KS}(\boldsymbol{\xi}), 0\} \geq 0$ and $q_e^i(\boldsymbol{\xi}) = \min\{\partial_e J_i^{KS}(\boldsymbol{\xi}), 0\} \leq 0$ and (L_e, U_e) , $e = 1, \dots, m$ are the moving asymptotes, such that $L_e < (x_e, \xi_e) < U_e$.

Once (33) is substituted into (32), the Lagrangian of the problem reads

$$\ell(\mathbf{x}, \lambda) = \widehat{J}_0^{KS}(\boldsymbol{\xi}) + \kappa \widehat{J}_1^{KS}(\boldsymbol{\xi}) + \sum_{e=1}^m \left[\frac{(U_e - \xi_e)^2 (p_e^0(\boldsymbol{\xi}) + \kappa p_e^1(\boldsymbol{\xi}))}{U_e - x_e} - \frac{(\xi_e - L_e)^2 (q_e^0(\boldsymbol{\xi}) + \kappa q_e^1(\boldsymbol{\xi}))}{x_e - L_e} \right] \quad (34)$$

where $\kappa \geq 0$ is the Lagrange multiplier. The stationarity condition of the Lagrangian with respect to x_e

$$\partial_e \ell(\mathbf{x}, \lambda) = \frac{(U_e - \xi_e)^2 (p_e^0(\boldsymbol{\xi}) + \kappa p_e^1(\boldsymbol{\xi}))}{(U_e - x_e)^2} + \frac{(\xi_e - L_e)^2 (q_e^0(\boldsymbol{\xi}) + \kappa q_e^1(\boldsymbol{\xi}))}{(x_e - L_e)^2} = 0 \quad (35)$$

can be solved explicitly, giving the primal update map

$$x_e(\kappa) = \max \left\{ \delta_-, \min \left\{ \delta_+, \frac{L_e(U_e - \xi_e) \sqrt{p_e^0(\boldsymbol{\xi}) + \kappa p_e^1(\boldsymbol{\xi})} + U_e(\xi_e - L_e) \sqrt{-q_e^0(\boldsymbol{\xi}) - \kappa q_e^1(\boldsymbol{\xi})}}{(U_e - \xi_e) \sqrt{p_e^0(\boldsymbol{\xi}) + \kappa p_e^1(\boldsymbol{\xi})} + (\xi_e - L_e) \sqrt{-q_e^0(\boldsymbol{\xi}) - \kappa q_e^1(\boldsymbol{\xi})}} \right\} \right\} \quad (36)$$

where $0 < \delta_- < \delta_+ < 1$ are the adaptive move limits, depending on the asymptotes and we have highlighted the dependence on the dual variable κ . This latter can be computed from the following equation, obtained by formally substituting (36) into (34) and imposing stationarity with respect to κ

$$\psi(\kappa) = \widehat{J}_1^{KS}(\boldsymbol{\xi}) + \sum_{e=1}^m \left[\frac{(U_e - \xi_e)^2 p_e^1(\boldsymbol{\xi})}{U_e - x_e(\kappa)} - \frac{(\xi_e - L_e)^2 q_e^1(\boldsymbol{\xi})}{x_e(\kappa) - L_e} \right] = 0 \quad (37)$$

The re-design procedure is implemented in the routine `ocUpdate`, listed at the bottom of this Section. The input parameters are the current re-design step (`loop`), the current design point, objective sensitivity, constraint value and sensitivity (`xT`, `dg0`, `g1`, `dg1`), the design variables at the two previous iterations (`x0ld`, `x0ld1`), and the current asymptotes (`as`). The input `ocPar=[move,asReduce,asRelax]` collects the steplength (`move`) and the two numbers used for tightening and relaxing the asymptotes according to the smoothness of the optimization history (`asReduce`, `asRelax`).

The evolution of the asymptotes and their link with the adaptive bounds δ_- and δ_+ (called `xL` and `xU`) are conceptually identical to that suggested by Svanberg (1987) (see lines 4-13). Following Guest et al (2011) we allow the tightening of the initial asymptotes to accommodate large β values, by passing this parameter to the `ocUpdate` routine. The user can also reset the asymptotes whenever continuation is applied on the penalization and projection parameters, by passing the additional variable `restartAsy`.

The primal update (36) and stationarity condition (37) are defined on lines 20-23, based on the positive variables `p0`, `q0`, `p1` and `q1`, representing $(U_e - \xi_e)^2 p_e^i$ and $-(\xi_e - L_e)^2 q_e^i$, $i = 0, 1$, respectively (lines 17-18). The dual variable κ , is computed between lines 26-33 accounting for three possible situations: given the search window $[0, \bar{\kappa}]$ (e.g. $\bar{\kappa} = 10^6$)

1. If $\psi(0)\psi(\bar{\kappa}) < 0 \rightarrow$ the Lagrange multiplier is within $(0, \bar{\kappa})$, and we compute it by the built-in Matlab function `fzero`, applying a version of the Brent's algorithm (Brent, 1973) (lines 27-28);
2. $\psi(0) < 0 \rightarrow$ the constraint is not active within the current local expansion. Thus, we set $\kappa = 0$ and $x_e = x_e(0)$ (line 30);
3. $\psi(\bar{\kappa}) > 0 \rightarrow$ the constraint cannot be fulfilled within the current local expansion (i.e. we cannot find a feasible solution). In this case, we set $\kappa = \bar{\kappa}$ and $x_e = x_e(\bar{\kappa})$ (line 32);

We stress that the present update rule can still be interpreted as an ‘‘OC-like’’ scheme since, for the simple case of a single constraint we are concerned with, the primal map (36) can be written out explicitly.

In our testing we have generally observed good behavior of this update rule. However, we acknowledge that the rather heuristic update for the special cases 2. and 3. may lead to oscillations in the convergence history, or even breakdowns. Since a robust optimizer is beyond the reach of a 35-lines optimization routine and beyond the purpose of this paper, the users who might face bad behavior of the `ocUpdate` are recommended to replace it with the MMA. As an example, considering the classic Matlab version of the MMA ‘‘mmasub’’ (Svanberg, 2007), the buckling maximization problem, with compliance and volume constraint can be solved by replacing lines 224-226 with the following

```

1 if loop==1, xOld=x(act); xOld1=xOld; low=[]; upp=[]; end
2 [xMMA,yy,zmma,lmid,xi,eeta,muu,zet,s1,low,upp]=mmasub_new(1,length(act),loop,x(act),max(x(act)-ocPar(1),0),...
3 min(x(act)+ocPar(1),1),xOld,xOld1,g0,dg0(act),0.,g1,dg1(act)',0,low,upp,aOMMA,aMMA,ccMMA,ddMMA,beta,restartAs)
4 xOld1 = xOld; xOld = x(act); x(act) = xMMA;

```

if the user still wants to consider a single, KS aggregated constraint. Alternatively, the following call

```

1 if loop==1, xOld=x(act); xOld1=xOld; low=[]; upp=[]; end
2 [xMMA,yy,zmma,lmid,xi,eeta,muu,zet,s1,low,upp]=mmasub_new(2,length(act),loop,x(act),max(x(act)-ocPar(1),0),...
3 min(x(act)+ocPar(1),1),xOld,xOld1,g0,dg0(act),0.,g1Vec,[dg1c(act)';dg1V(act)'],0,low,upp,aOMMA,aMMA,ccMMA,...
4 ddMMA,beta,restartAs)
5 xOld1 = xOld; xOld = x(act); x(act) = xMMA;

```

can be used for treating the two constraints separately. The parameters `aOMMA`, `aMMA`, `ccMMA` and `ddMMA` can be selected as recommended in (Svanberg, 2007).

```

1 function [x,as,lmid]=ocUpdate(loop,xT,dg0,g1,dg1,ocPar,xOld,xOld1,as,beta)
2 % ----- definition of asymptotes and move limits
3 [xU,xL] = deal(min(xT+ocPar(1),1), max(xT-ocPar(1),0));
4 if (loop<2.5 || restartAsy==1)
5     as = xT+[-0.5,0.5].*(xU-xL)./(beta+1);
6 else
7     tmp = (xT-xOld).*(xOld-xOld1);
8     gm = ones(length(xT),1);
9     [gm(tmp>0), gm(tmp<0)] = deal(ocPar(3),ocPar(2));
10    as = xT + gm .* [-(xOld-as(:,1)),(as(:,2)-xOld)];
11 end
12 xL = max(0.9*as(:,1)+0.1*xT,xL); % adaptive lower bound
13 xU = min(0.9*as(:,2)+0.1*xT,xU); % adaptive upper bound
14 % ----- split (+) and (-) parts of the objective and constraint derivatives
15 p0_0 = (dg0>0).*dg0; q0_0 = (dg0<0).*dg0;
16 p1_0 = (dg1>0).*dg1; q1_0 = (dg1<0).*dg1;
17 [p0,q0] = deal(p0_0.*(as(:,2)-xT).^2,-q0_0.*(xT-as(:,1)).^2);
18 [p1,q1] = deal(p1_0.*(as(:,2)-xT).^2,-q1_0.*(xT-as(:,1)).^2);
19 % ----- define the primal projection map and dual function
20 primalProj = @(lm) min(xU,max(xL,(sqrt(p0+lm*p1).*as(:,1)+sqrt(q0+lm*q1).*as(:,2))...
21 ./ (sqrt(p0+lm*p1)+sqrt(q0+lm*q1))));
22 psiDual = @(lm) g1 - ( (as(:,2)-xT)'*p1_0 - (xT-as(:,1))*q1_0 ) + ...
23 sum(p1./ (max(as(:,2)-primalProj(lm),1e-12)) + q1./ (max(primalProj(lm)-as(:,1),1e-12)));
24 % ----- compute the Lagrange multiplier through bisection
25 lmUp = 1e6; x = xT; lmid = -1;
26 if psiDual(0) * psiDual(lmUp) < 0 % check if LM is within the interval
27     lmid = fzero(psiDual, [0, lmUp]);
28     x = primalProj(lmid); % update desing variables
29 elseif psiDual(0) < 0 % constraint cannot be active
30     lmid=0; x=primalProj(lmid);
31 elseif psiDual(lmUp) > 0 % constraint cannot be fulfilled
32     lmid=lmUp; x=primalProj(lmid);
33 end
34 end

```

B.1 Some properties of the KS function

Given the set of functions $\{g_i(\mathbf{x})\}_{i=1,\dots,q}$, where each $g_i: \mathbb{R}^m \rightarrow \mathbb{R}$ is not necessarily smooth, we can build the smooth Kreisselmeier-Steinhauser (KS) aggregation function (Kreisselmeier and Steinhauser, 1979)

$$J^{KS}[g_i](\mathbf{x}) = g_*(\mathbf{x}) + \frac{1}{\rho} \ln \left(\sum_{i=1}^q e^{\rho(g_i(\mathbf{x}) - g_*(\mathbf{x}))} \right) \quad (38)$$


```

230 if any(prSel{1} == 'B') % plot design, g0 & g1 evolution, BLFs evolution
231     subplot(2,2,1:2);
232     colormap(gray); imagesc(1-reshape(xPhys,nely,nelx));
233     caxis([0,1]); axis equal; axis off; drawnow; title('Current design');
234     subplot(2,2,3)
235     yyaxis left; plot(1:loop,plotL); ylabel(strL);
236     yyaxis right; plot(1:loop,plotR); ylabel(strR); title('Objective and constraint');
237     subplot(2,2,4)
238     plot(1:loop,1./muVec(:,1:4)); title('Lowest BLFs');
239 else % plot the current design only
240     colormap(gray); imagesc(1-reshape(xPhys,nely,nelx));
241     caxis([ 0,1]); axis equal; axis off; drawnow;
242 end
243 % apply continuation on penalization(s), beta & aggregation parameter(s)
244 penalKold = penalK; penalGold = penalG; betaOld = beta;
245 [penalK,penalG,beta,pAgg] = deal(cnt(penalK, penalCntK, loop), ...
246     cnt(penalG,penalCntG,loop), cnt(beta,betaCnt,loop), cnt(pAgg,pAggCnt,loop));
247 if (beta-betaOld~= 0 || penalK-penalKold~=0 || penalG-penalGold~=0)
248     restartAs = 1; else, restartAs = 0; end % restart asymptotes if needed
249 end
250 end

```